J Mater Sci (2008) 43:6459–6467
DOI 10.1007/s10853-008-2979-1

Orientational distribution of parent–daughter structure of isotactic polypropylene: a study using simultaneous synchrotron WAXS and SAXS

Peng-Wei Zhu · Graham Edward

Received: 11 May 2008 / Accepted: 2 September 2008 / Published online: 20 September 2008

Abstract The molecular and lamellar orientations of injection-moulded isotactic polypropylene were investigated using simultaneous wide- and small-angle X-ray scatterings. In order to obtain the meaningful degree of molecular orientation with respect to the flow direction, the axis orientations of parent and daughter lamellae were separately calculated. The molecular orientation of thin material is consistent with the lamellar orientation. However, the decrease in the lamellar orientation of thick material is associated with a constant degree of molecular orientation, which would indicate an intra slip between parent lamellae along the flow direction.

Introduction

The isotactic polypropylene (iPP) is one of the most important engineering polymers. iPP can form a skin–core structure in the processing of injection moulding [1–8]. The skin region is very thin with a very high content of amorphous due to a rapid cooling rate. The lower cooling rate in the core region allows a complete relaxation of chain molecules and consequently a growth of spherulites. The skin and core regions are separated by a shear region in which a branched shish-kebab structure forms [9–13]. Figure 1 schematically shows the branched shish-kebab structure and schematic 2-D X-ray patterns. The special feature of branched shish-kebab is a mixed bimodal orientation, i.e. the *c*-axis of parent lamellae is preferentially oriented to the flow direction, whereas the *c*-axis of daughter lamellae is preferentially perpendicular to the flow direction. The daughter lamellae are considered to grow epitaxially on the formed parent lamellae with an approximately ±80° [9].

Although the branched shish-kebab of iPP has been extensively studied, the molecular or axis orientation obtained always contains the contributions both from the parent and the daughter lamellae. Since the *c*- and *a**-axes of daughter lamellae are almost perpendicular to the counterparts of parent lamellae, the contributions from parents and daughters to the axis orientation can be cancelled each other. This would be particularly significant when the concentrations of parents and daughters are not negligible. For example, even if the *c*-axis highly orientates to the flow direction, the Hermans orientation function [14] can be very small or even negative [3, 15]. As a consequence, the physical nature of molecular orientation becomes ambiguous. In this article, we report on the orientations of injection-moulded iPP using simultaneous wide- and small-angle X-ray scattering (WAXS and SAXS). The Hermans orientation function of parent and daughter lamellae will be separately calculated. The molecular orientation obtained from WAXS is further confirmed by the lamellar orientation obtained from SAXS. The distributions of orientation with respect to the flow direction can be thus meaningfully constructed, which provides useful information on the morphological design and surface control.

Experimental

An iPP (Borealis HD601CF) was provided by Borealis. The average weight and number molecular weights are

P.-W. Zhu (✉) · G. Edward
Department of Materials Engineering, Cooperative Research Center for Polymers, Monash University, Clayton, VIC 3800, Australia
e-mail: peng.zhu@eng.monash.edu.au

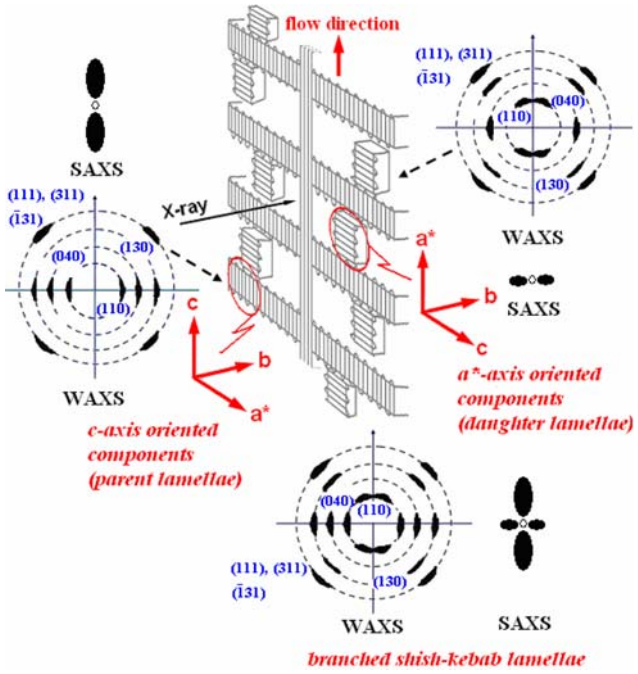

Fig. 1 A schematic diagram of branched shish-kebab structure and possible 2-D WAXS and SAXS patterns according to Ref. [3]

367,000 and 74,000, respectively. Rectangular plates of iPP were injection moulded with moulding conditions as follows: melt temperature 200 °C, mould temperature 40 °C, holding pressure 30 MPa, cooling time 15 s and flow front velocity 2 cm/s through the cavity. The width and length of plates are 73 and 120 mm with the thicknesses of 1.1 and 4.9 mm, respectively.

The synchrotron experiments were performed at the Australian National Beamline Facility (ANBF) in Tsukuba, Japan. The details can be referred to the previous work [15]. In brief, the ANBF is installed on a bending magnet port, and delivers monochromatic synchrotron X-rays in the energy range 4.5–20 keV to the experimental station in a hutch. The instrument has a multi-configuration vacuum diffractometer that uses image plates as its detector system. The square-shaped beam with the wavelength of 2.0 Å had a dimension of 200 × 200 μm^2. The scattered intensity through a hole on a WAXS image plate was recorded by an SAXS image plate. Figure 2 shows the schematic diagram of experimental setup.

The specimens were cut at a centre position of 60 mm away from the gate of plates. The specimen surface was parallel to the flow direction. The specimens were mounted at a position which was, 118 mm from WAXS image plate and 962 mm from SAXS image plate. Measurements were performed with the primary beam being perpendicular to the flow direction. The beam passed through the specimen and the illuminated zone was changed with a vertical shift of the sample holder along the direction of plate thickness (or specimen width). Only one half width of each specimen was illuminated on the assumption that the morphology at the same distance from the surfaces of a plate is the same. Scattering without the specimen was recorded as a background.

Results and discussion

Figure 3 shows 2-D WAXS patterns at different distances from the surface. At a given position, the reflections of thin material show a much stronger azimuthal dependence than those of thick one, indicating the higher degree of molecular orientation, as expected. Especially, the branched shish-kebab structure observed from (110) reflection appears in the different ranges of distance. For example, the bimodal feature is significant at 400 μm of thin material, but not distinguishable at 300 μm of thick material. Figure 4 shows 2-D SAXS patterns simultaneously recorded with WAXS. The patterns are partially obscured by the beam stop. The stacks of parent lamellae give the meridional scattering from SAXS patterns, whereas the stacks of daughter lamellae give the equatorial scattering. It should be pointed out, however, that the shish also gives the scattering alone the equatorial direction. The interpretation of equatorial scattering of SAXS is therefore difficult due to the overlap of scattering from daughter lamellae and shishes. As will be seen, we only calculate the parameters of parent lamellae. The narrower spots of meridional scattering indicate the higher degree of lamellar orientation.

In order to elucidate the distance dependence of molecular orientation, the azimuthal profiles of (110) are illustrated in Fig. 5. The bimodal (110) reflection has been well explained [5, 9–13]. The oriented structure has the parent and daughter, respectively, in the areas around the azimuthal angle φ of 90 (or −90°) and 0°. The molecular orientation is estimated using the Hermans orientation function by [14]:

$$f_H = \frac{3\langle\cos^2\varphi\rangle - 1}{2} = \frac{3\int_0^{\pi/2} I(\varphi)\cos^2\varphi\sin\varphi\,d\varphi}{2\int_0^{\pi/2} I(\varphi)\sin\varphi\,d\varphi} - \frac{1}{2}. \quad (1)$$

The orientation function $f_H = 1$ when an axis is perfectly parallel to the reference direction, −0.5 when an axis is perfectly perpendicular to the reference direction and 0 when an axis is randomly distributed. The baselines shown in Fig. 5 were used in the calculations. Assuming the rotational symmetry around the flow direction and defining the angles of *a**-, *b*- and *c*-axes with the flow direction, the sum of the orientation functions can be given as follows:

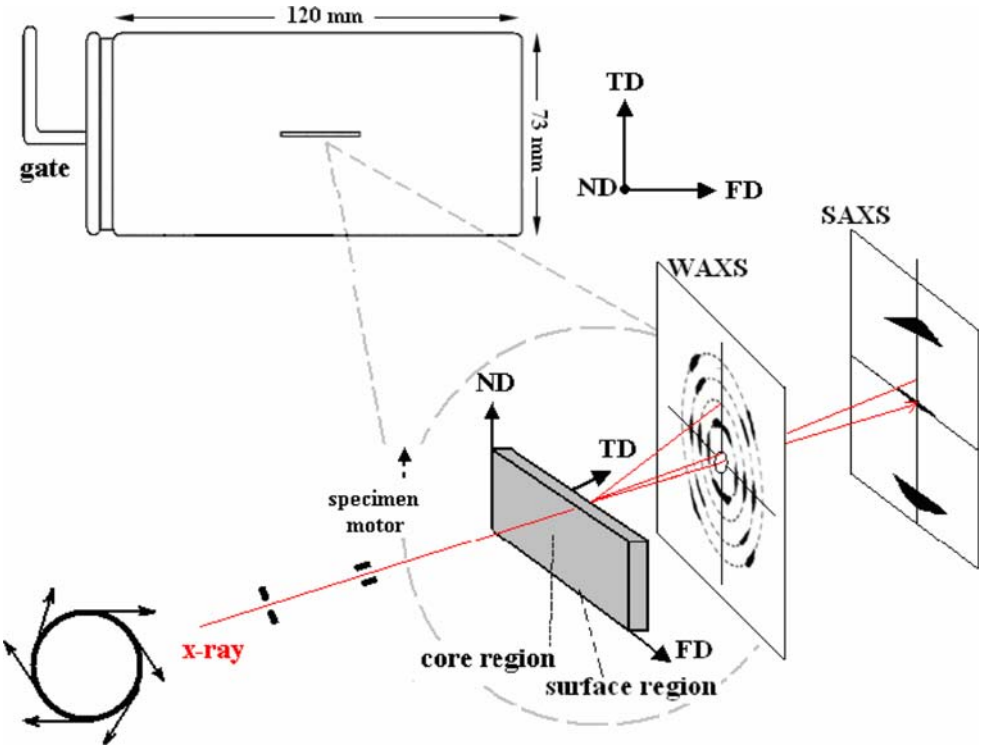

Fig. 2 A schematic diagram of simultaneous synchrotron WAXS and SAXS experiments. FD, direction along the flow; TD, direction traverse to the flow; ND, direction normal to the flow and the plate surface

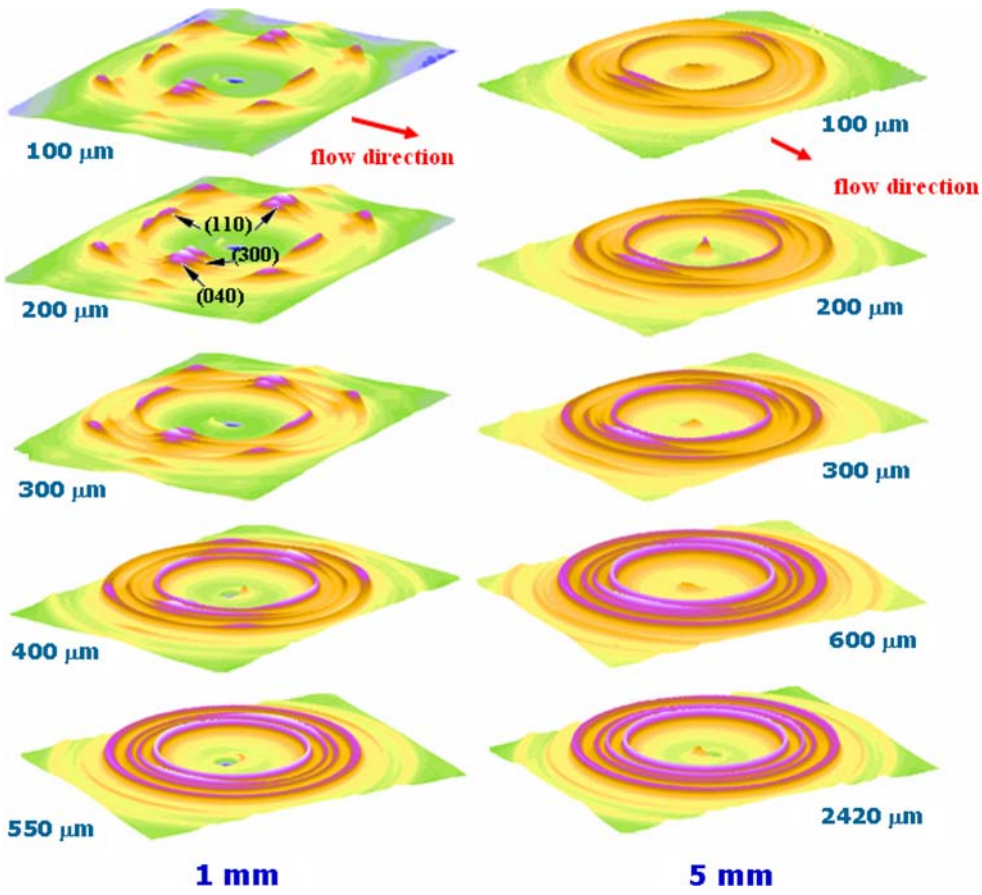

Fig. 3 Distributions of 2-D WAXS patterns through the thickness of iPP plates

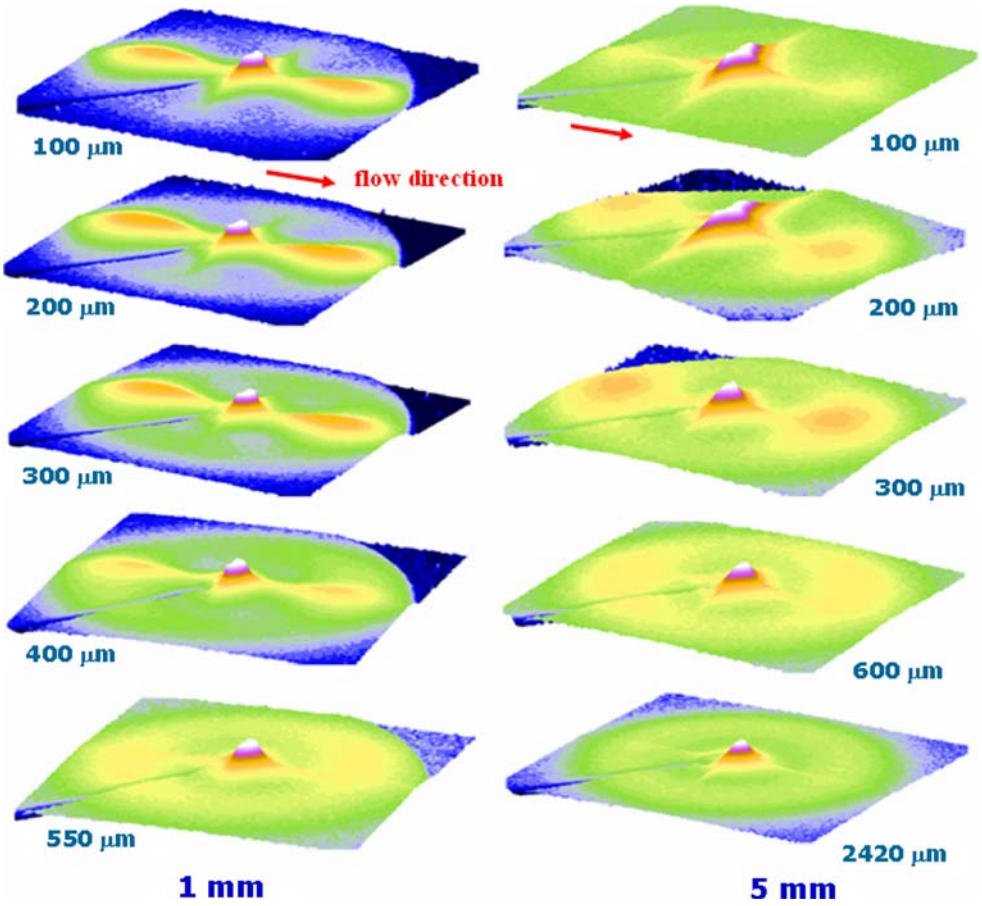

Fig. 4 Distributions of 2-D SAXS patterns through the thickness of iPP plates

$$f_{a^*} + f_b + f_c = 0. \quad (2)$$

For the α-form crystal, the *b*-axis orientation function f_b is directly calculated from the (040) reflection, whereas the *c*-axis orientation function f_c should be calculated from the (110) and (040) reflections using Wilchinsky's method as follows [16]:

$$\langle \cos^2 \sigma \rangle = 1 - 1.099 \langle \cos^2 \varphi_{(110)} \rangle - 0.901 \langle \cos^2 \varphi_{(040)} \rangle. \quad (3)$$

The *a**-axis orientation function f_{a^*} is then calculated by Eq. 2.

Figure 6a shows the distributions of f_b. Note that the *b*-axes of parents and daughters are all oriented along the same direction, or they are preferentially perpendicular to the flow direction. The thin material in general has the higher degree of *b*-axis orientation, particularly at 100 and 200 μm. The *b*-axis orientation of thin material decreases with increasing distance, whereas the *b*-axis orientation of thick material is rather scattered.

Figure 6b, c shows the distributions of f_c and f_{a^*} calculated from the whole azimuthal curves. As the distance from surface is increased, f_c sharply decreases form ~0.62 to ~−0.1, whereas f_{a^*} sharply increases from ~−03 to ~0.4. The data seem to be reasonable, within the experimental error, because they could be explained as the effect of shear flow on the axis orientation through the thickness. However, as mentioned above, f_c and f_{a^*} of branched shish-kebab structure can be interfered by the parent-to-daughter ratio or bimodal. Consequently, the molecular orientation with respect to the flow direction is unclear or even meaningless. For example, the value of f_{a^*} is 0 at 300 μm of thin material, which means a random distribution. However, the SAXS pattern at the same position indicates that the crystalline lamellae are highly oriented (see Fig. 4). Obviously, the axes should not be randomly distributed within the highly oriented lamellae.

In order to exclude the effect of parent-to-daughter ratio on the orientation functions, f_c and f_{a^*} were separately calculated from the areas corresponding to parents and daughters. The results are shown in Fig. 7. Apparently, the different distributions of molecular orientation are obtained. In the bimodal region, the *c*-axis of parents is highly oriented to the flow direction: f_c of thin material is a constant (~0.9) from 100 to 200 μm and then slightly decreases (~0.78) from 200 to 400 μm, whereas f_c of thick material is a constant (~0.79) from 100 to 300 μm. In the bimodal region, the *a**-axis of parents is highly

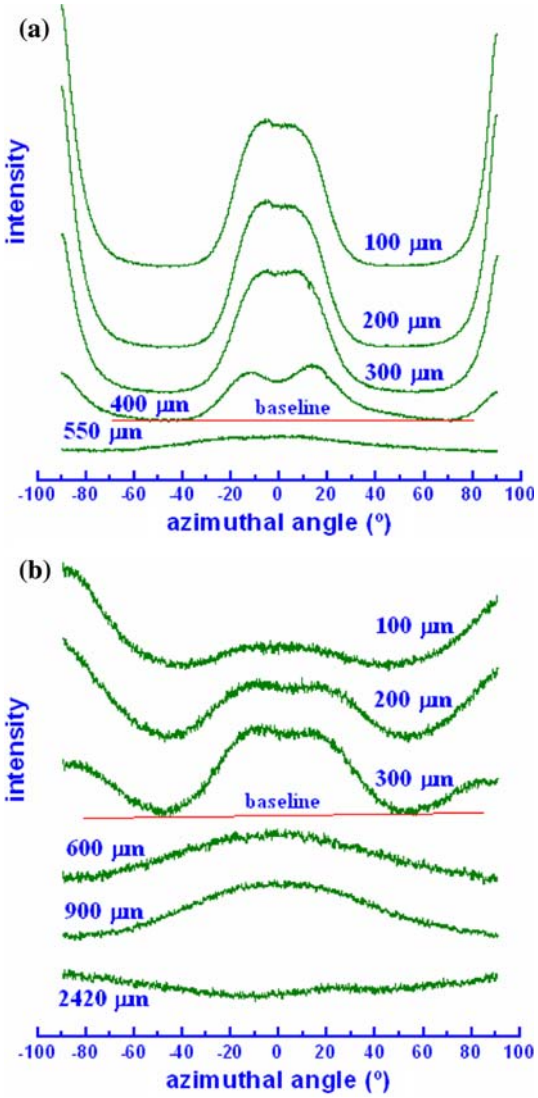

Fig. 5 Distributions of azimuthal profiles of (110) reflection through the thickness of iPP plates: (**a**) 1 mm plate, (**b**) 5 mm plate. The baselines were used in the calculation of orientation function. The flow direction is vertical

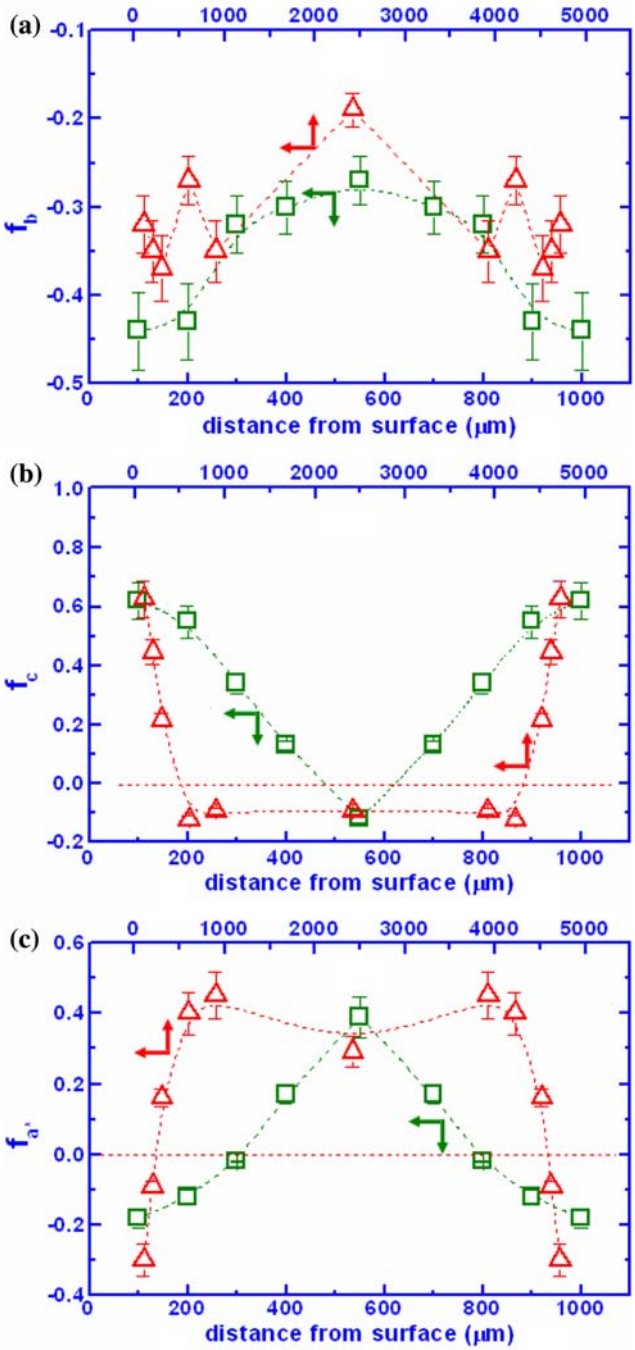

Fig. 6 Distributions of molecular orientation functions calculated from the whole curves shown in Fig. 5. (**a**) f_b, (**b**) f_c and (**c**) f_{a^*}. □, 1 mm; △, 5 mm

perpendicular to the flow direction with f_{a^*} values between -0.42 and 0.48. The continuous increase in f_{a^*} with the distance is not observed. Particularly, at 300 μm of thin material, $f_c = 0.78$ and $f_{a^*} = -0.48$, rather than $f_c = 0.14$ and $f_{a^*} = 0$ as obtained from the whole curve.

Figure 8 shows the distribution of molecular orientation in the daughters. In general, the c- and a^*-axes of daughters are highly oriented, though the bigger error was introduced in the calculation. The daughter lamellae are usually considered to be poorly defined crystalline stacks. The present results reveal that the daughters can be well oriented near the surface.

A relative comparison between parent lamellae and daughter lamellae can be made from the calculation of the fraction of daughter lamellae, $[A^*]$. This can be evaluated from azimuthal curves of the (110) reflection (see Fig. 5) according to Fujiyama et al. [3]:

$$[A^*] = \frac{A^*}{A^* + C}, \tag{4}$$

where A^* is the area around the azimuthal angle of 0° and C the area around 90°. Figure 9 indicates that the fraction

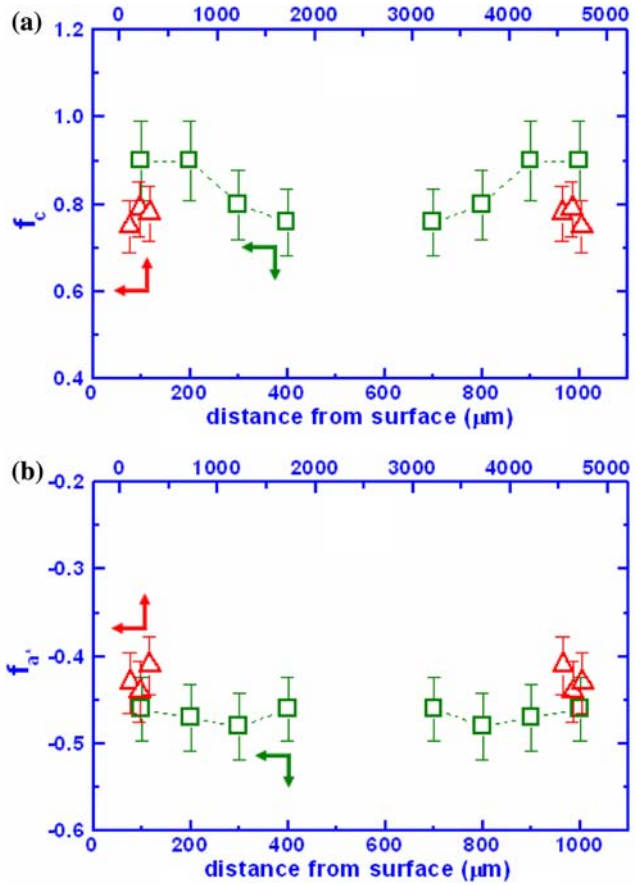

Fig. 7 Distributions of molecular orientations calculated from the areas corresponding to parent lamellae. (**a**) f_c and (**b**) f_{a^*}. □, 1 mm; △, 5 mm

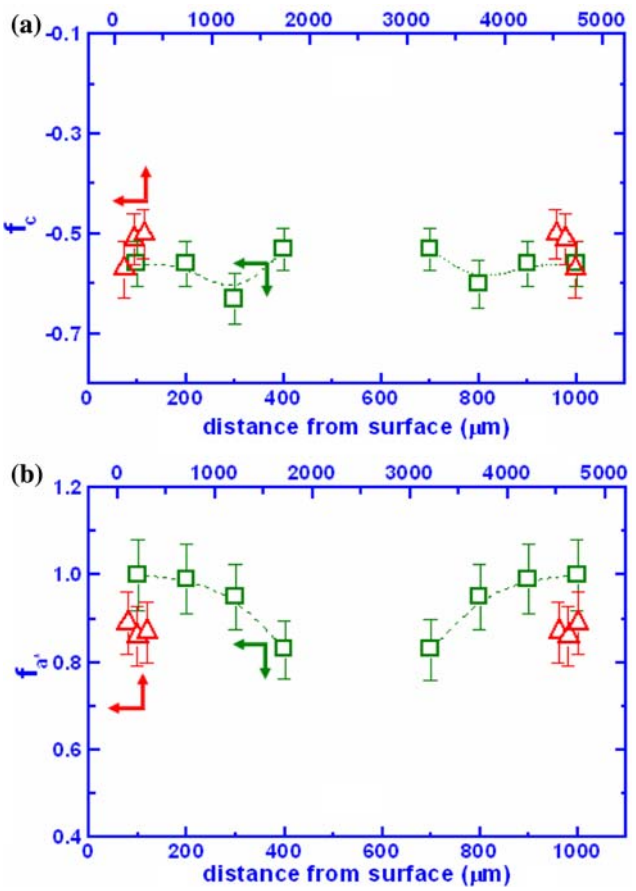

Fig. 8 Distributions of axial or molecular orientations calculated from the areas corresponding to daughter lamellae. (**a**) f_c and (**b**) f_{a^*}. □, 1 mm; △, 5 mm

of daughter lamellae increases with increasing the distance from the surface, which is in a good agreement with the literature [17].

Figure 10 shows the azimuthal profiles of meridional SAXS scattering (or from the parent lamellae). A relative level of lamellar orientation is obtained from the full width at half-maximum (FWHM) of azimuthal profiles. The lamellar orientation can also be evaluated by Hermans orientation function f [18]. Figure 11 shows the distributions of these orientation parameters through the thickness.

For the thin material, FWHM slightly increases or f slightly decreases as the distance is increased, which corresponds to the slight decrease in the c-axis orientation f_c. This is understandable because the lamellar orientation is related to the molecular orientation in a way that the direction of parent lamellae is parallel to the c-axis. Note that at 300 μm of thin material the high level of lamellar orientation is obtained from the parent lamellae, which is in a good agreement with the high level of molecular orientation at the same position, as shown Fig. 7.

For the thick material, on the other hand, the continuous increase in FWHM (from 100 to 300 μm) is related to a

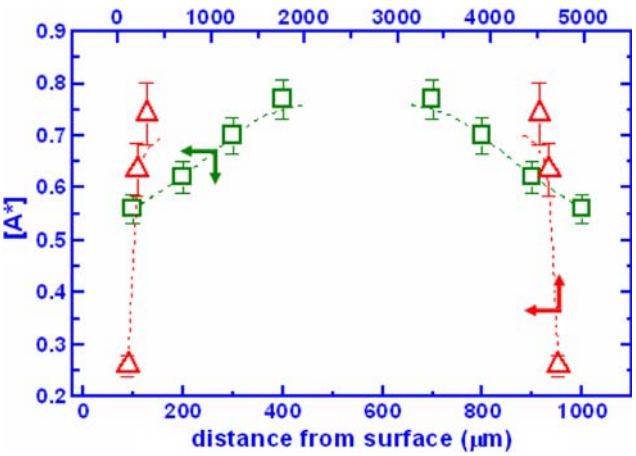

Fig. 9 Distribution of fraction of daughter lamellae [A^*]. □, 1 mm; △, 5 mm

constant f_c as shown in Fig. 7a. This is interesting because the results suggest that the parent lamellae as a whole decline away from the flow direction, but the fold chains within the lamellae remain the same degree of molecular orientation. The observation would be explained as the

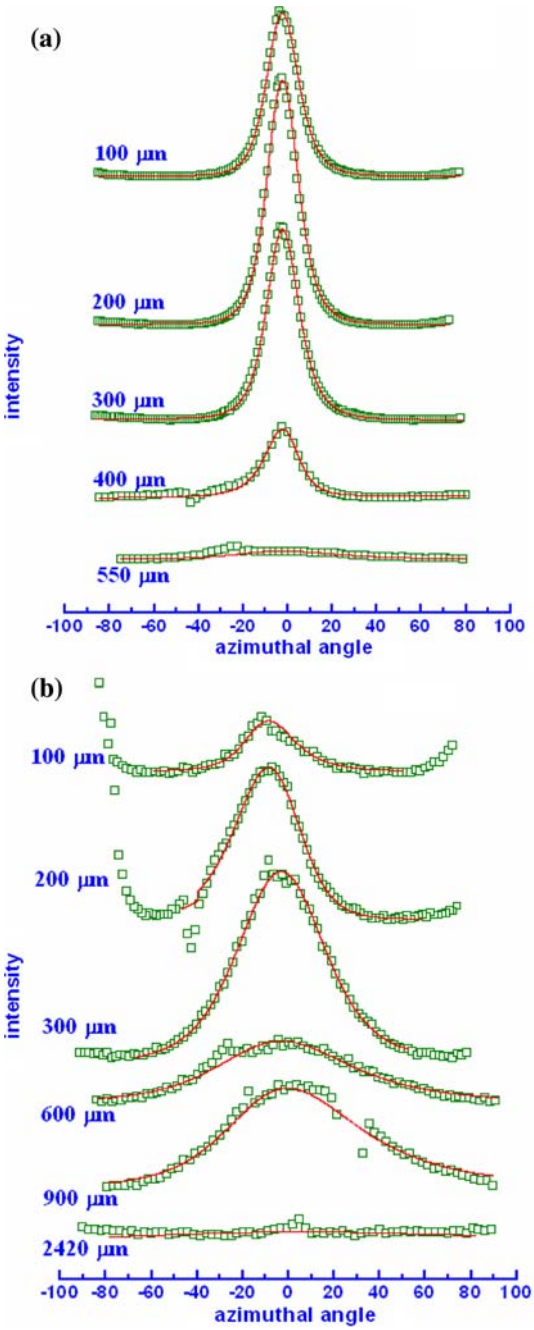

Fig. 10 Distributions of SAXS azimuthal profiles of parent lamellae through the thickness of iPP plates. (**a**) 1 mm, (**b**) 5 mm. The flow direction is vertical

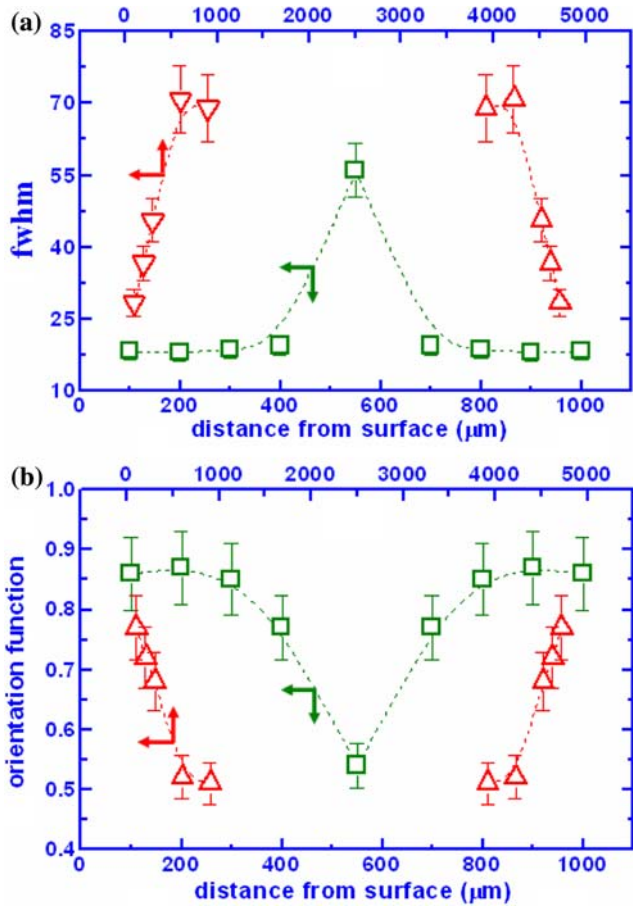

Fig. 11 (**a**) FWHM distributions of SAXS azimuthal profiles of parent lamellae. (**b**) Distributions of orientation function *f* of parent lamellae. (**c**) Schematic illustrations of kebab structures in thin and thick plates. □, 1 mm; △, 5 mm

lamellar slip [19] within individual parent lamellae of thick material during the moulding processing, which can be schematically shown in Fig. 12.

The stretched segments and coil chains are expected to coexist under supercooling [20]. The stretched segments crystallize instantaneously into the shishes and then the coil chains crystallize into the kebabs on the formed shishes. The shish-kebab structure is a hierarchical crystalline assembly, which would include centrally stretched-chain microshishes, partially stretched-chain macroshishes, microkebabs and macrokebabs [7, 21–24]. The microkebabs would be intrinsically implanted into the shishes and the macrokebabs grow on the surface of formed microkebabs. At a given position, the thick material has the higher temperature for the crystallization and the longer time for the solidification. At high temperatures, the forthcoming coil chains may have more freedom to deposit onto anywhere of the surfaces of formed microkebab in forming the macrokebabs. As a result, the structure of whole kebabs is not continuous. If the cooling rate is high enough, like the thin material, the second growth of the kebabs would not take place before the solidification completes. The structure of the kebabs is thus continuous microkebabs. Since the microkebabs are thermally more stable than the macrokebabs [24], the different properties are expected in the bimodal region.

Note that the hierarchical structure of kebabs could be compatible with the formation of possible lamellar blocks

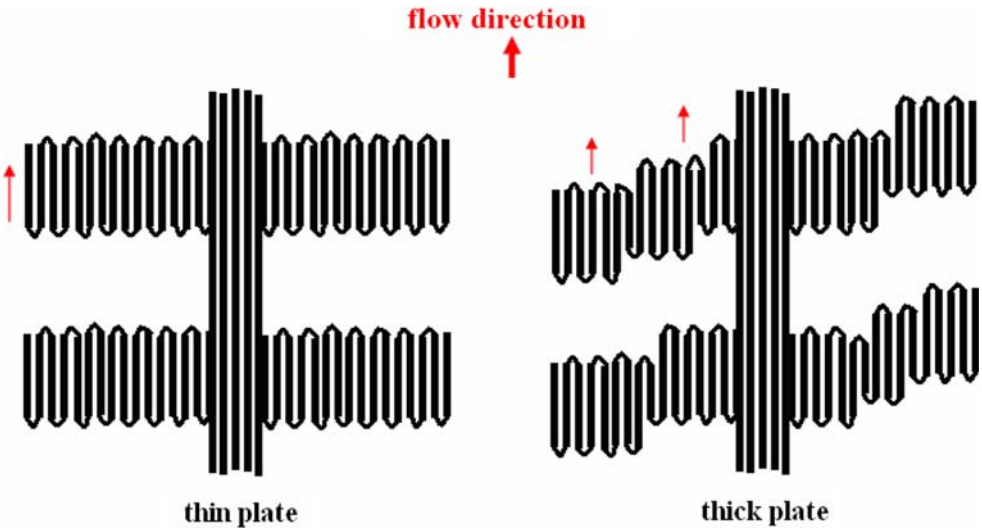

Fig. 12 Schematic illustrations of parent lamellae in thin and thick plates. □, 1 mm; △, 5 mm

in the polymer crystallization [25–27]. The formation of a crystalline lamella is suggested to go consecutively through three steps. The first step is the formation of imperfect mesomorphic blocks, followed by a relaxation process which transfers the mesomorphic blocks into granular blocks. The granular blocks are finally merged into a crystalline lamella. Accordingly, even if an individual kebab is a continuous component, its structure would be consisted of consecutive blocks with boundaries. The structural details can be tuned by the cooling rate in the moulding operation.

Conclusion

The orientational distributions of injection-moulded iPP were investigated using the simultaneous WAXS and SAXS. The upper limits where the bimodal feature is observed are 400 μm for the thin material and 300 μm for the thick material. In order to obtain the meaningful level of molecular orientation with respect to the flow direction, the axis orientations of parent and daughter lamellae were separately calculated. In the thin material, the orientations of *c*- and *a**-axes of parents slightly decrease with the distance from 100 to 400 μm, which corresponds to the decrease in the lamellar orientation. In the thick material, however, the orientations of *c*- and *a**-axes of parent lamellae are constant from 100 to 300 μm, which corresponds to the successive decrease in the lamellar orientation. On the basis of these observations, it is proposed that the parent lamellae in the thin material are consisted of microkebabs, whereas the parent lamellae in the thick material are consisted of microkebabs and macrokebabs. These parent lamellae in the thick material would be intra slip along the flow direction. It is also found that the daughter lamellae are not poorly defined crystalline stacks. The molecular orientation within the daughter lamellae can be well oriented in the present work.

Acknowledgements This work was performed at the Australian National Beamline Facility (ANBF) with support from the Australian Synchrotron Research Program, which is funded by the Commonwealth of Australia under the Major National Research Facilities Program. The authors are grateful to Dr. James Hester of ANSTO and Dr. Peter Farrington of Moldflow for their help in the experiments.

References

1. Stern C, Frick A, Weickert G (2007) J Appl Polym Sci 103:519. doi:10.1002/app.24156
2. Katti SS, Schultz J (1982) Polym Eng Sci 22:1001. doi:10.1002/pen.760221602
3. Fujiyama M, Wakino T, Kawasaki Y (1988) J Appl Polym Sci 35:129. doi:10.1002/app.1988.070350104
4. Zipper P, Janosi A, Wrentschur E, Abuja PM (1991) J Appl Cryst 24:702. doi:10.1107/S0021889891001917
5. Na B, Fu Q (2002) Polymer 43:7367. doi:10.1016/S0032-3861(02)00637-7
6. Zhang W, Martins JA (2007) Polymer 48:6215. doi:10.1016/j.polymer.2007.08.029
7. Eder G, Janeschitz-Kriegl H (1997) Mater Sci Technol 18:268
8. Ogino Y, Fukushima H, Takahashi N, Matsuba G, Nishida K, Kanaya T (2006) Macromolecules 39:7617. doi:10.1021/ma061254t
9. Lotz B, Wittmann C, Lovinger A (1996) Polymer 37:4979. doi:10.1016/0032-3861(96)00370-9
10. Dean DM, Rebenfeld L, Register RA, Hsiao BS (1998) J Mater Sci 33:4797. doi:10.1023/A:1004474128452
11. Assouline E, Wachtel E, Grigull S, Lustiger A, Wagner HD, Marom G (2001) Polymer 42:6231. doi:10.1016/S0032-3861(01)00087-8
12. Zhang S, Minus ML, Zhu L, Wong C, Kumar S (2008) Polymer 49:1356. doi:10.1016/j.polymer.2008.01.018
13. Nozue Y, Shinohara Y, Ogawa Y, Sakurai T, Hori H, Kasahara T et al (2007) Macromolecules 40:2036. doi:10.1021/ma061924v

14. Alexander LE (1969) X-ray diffraction methods in polymer science. Wiley, NY
15. Zhu PW, Tung J, Phillips A, Edward G (2006) Macromolecules 39:1821. doi:10.1021/ma052375g
16. Wilchinsky ZW (1960) J Appl Phys 31:1969. doi:10.1063/1.1735481
17. Schrauwen BAG, Breemen LCAv, Spoelstra AB, Govaert LE, Peters GWM, Meijer HEH (2004) Macromolecules 37:8618. doi:10.1021/ma048884k
18. Keates P, Mitchell GR, Peuvrel-Disdier E, Navard P (1993) Polymer 34:1316. doi:10.1016/0032-3861(93)90792-9
19. Wang Y, Na B, Zhang Q, Tan H, Xiao Y, Li L et al (2005) J Mater Sci 40:6409. doi:10.1007/s10853-005-1746-9
20. Dukoski I, Muthukumar M (2003) J Chem Phys 118:6648. doi:10.1063/1.1557473
21. Hill MJ, Keller A (1981) Colloid Polym Sci 259:335. doi:10.1007/BF01524712
22. Koscher E, Fulchiron R (2002) Polymer 43:6931. doi:10.1016/S0032-3861(02)00628-6
23. Liu T, Petermann J, He C, Liu Z, Chung T (2001) Macromolecules 34:4305. doi:10.1021/ma010380o
24. Zuo F, Keum JK, Yang L, Somani RH, Hsiao B (2006) Macromolecules 39:2209. doi:10.1021/ma052340g
25. Strobl G (2000) Eur Phys J E3:165
26. Hiss R, Hoberika S, Lynn C, Strobl G (1999) Macromolecules 32:4390. doi:10.1021/ma981776b
27. Men Y, Rieger J, Strobl G (2003) Phys Rev Lett 91:095502. doi:10.1103/PhysRevLett.91.095502